University of Bath

Alternative formats
If you require this document in an alternative format, please contact:
openaccess@bath.ac.uk

Unsteady Lift and Moment of a Periodically Plunging Airfoil

N. Chiereghin, D. J. Cleaver and I. Gursul

University of Bath, Bath, BA2 7AY, United Kingdom

To simulate the effects of gusts and maneuvers, lift, moment and flow measurements are presented for a periodically plunging airfoil at a Reynolds number of 20,000 over a wide range of reduced frequency ($k \leq 1.1$), amplitude ($A/c \leq 0.5$) and mean angle of attack (0°to 20°). For this parameter range, maximum lift in the cycle is determined by the circulatory lift, regardless of whether a leading-edge vortex (LEV) is formed or not, whereas maximum nose-down moment is determined by the competition between the added-mass and the arrival of the LEV near the trailing-edge. The LEV generally increases mean lift and decreases mean moment. This increase, which is not predicted well by the reduced-order models, correlates with the maximum effective angle of attack of the motion, rather than the Strouhal number. In contrast, the amplitude and phase of lift are predicted well by the Theodorsen theory, whether LEVs present or not. Hence, LEVs have minimal effect on the fluctuating lift. However, the amplitude of the pitching moment is not predicted well by the Theodorsen theory, if LEVs are present. The competition between the added-mass and LEV causes the non-monotonic variation of the moment amplitude as a function of reduced frequency.

Nomenclature

A	=	peak-to-peak amplitude, $2a$
a	=	plunging amplitude
a_0	=	time-averaged lift coefficient
a_1	=	first harmonic of lift coefficient fluctuations
b	=	wing span
c	=	chord
C_l	=	lift coefficient, $l/0.5\rho U_\infty^2 cb$
C_m	=	pitching moment coefficient at ¼ chord, $M/0.5\rho U_\infty^2 cbc$
f	=	plunging frequency
FFT	=	fast Fourier transform
GK	=	Goman-Khrabrov method
h	=	plunging motion coordinate
k	=	plunging reduced frequency, $\pi f c/U_\infty = \pi St_c$
l	=	lift force
M	=	pitching moment at ¼ chord
LDVM	=	LESP-based Discrete Vortex Method
LESP	=	Leading Edge Suction Parameter
LB	=	Leishman-Beddoes method
Re	=	Reynolds number, $\dfrac{\rho U_\infty c}{\mu}$
St_c	=	Strouhal number based on chord, $f c/U_\infty$
St_A	=	Strouhal number based on amplitude
T	=	plunge period
U_{pl}	=	plunge velocity
U_∞	=	freestream velocity
α	=	geometric angle of attack
α_{eff}	=	effective of attack, $\alpha + \tan^{-1}\left(U_{pl}/U_\infty\right)$
Φ	=	phase lag
ω	=	span-wise vorticity

I. Introduction

Unsteady aerodynamics of oscillating airfoils has received substantial interest for its numerous applications, which include micro air vehicles [1], biologically inspired flows [2, 3], helicopter blades [4], and aircraft wing loads due to unsteady wing motion [5], turbulence and gusts [6]. Range of frequency and amplitude as well as type of kinematic motion may widely vary in these applications. For low frequency and amplitude, the flow remains mostly attached. However, with increasing frequency or amplitude, separation becomes prevalent and concentrated leading-edge and trailing edge vortices start to shed. There is a need for greater understanding of these unsteady flow fields which are characterized by massive separation and vortical disturbances, and for methods that can predict the unsteady forces and moments. The prediction of the unsteady lift/moment is important for aircraft design at all scales. For example, the structure of civil aircraft is designed to withstand the most extreme unsteady lift experienced during gust encounters or extreme maneuvers no matter how rare their occurence. It is therefore necessary to have models capable of predicting peak loads during these extreme conditions. Current numerical simulations require unrealistic computational resources for the range of extreme flight conditions. As a consequence, high safety factors are applied during the design process. Since these extreme cases dictate the structural requirements, this often produces a substantial increase in the weight of aircraft.

The main focus of this article is the unsteady lift and pitching moment. For airfoils the oscillating motion can be plunging, pitching or surging; for the purposes of this article we are concerned with plunging motion. Pure plunging motion is simpler, yet fundamental, and an approximate simulation of vertical gusts. The effective angle is the sum of the geometric angle of attack α (which remains constant) and the motion-induced angle of attack,

$$\alpha_{\text{eff}} = \alpha + \tan^{-1}(U_{pl}/U_\infty), \tag{1}$$

where U_{pl} is the plunge velocity and U_∞ is the freestream velocity. The salient parameters for plunging airfoils are the geometric angle of attack α, the plunging frequency f, and the peak-to-peak plunging amplitude A. If the flow is attached the most significant dimensionless group is the Strouhal number based on the amplitude $St_A = fA/U_\infty$. This is a ratio of the plunge velocity to the freestream velocity and is therefore directly related to the maximum effective angle of attack. At high effective angles of attack the flow becomes separated and a second parameter becomes

significant: reduced frequency, $k = \pi f c / U_\infty$ [7] (Strouhal number based on the chord length St_c is also used in the literature, $k = \pi St_c$).

As the mean angle of attack, frequency and amplitude are increased, the relative roles of the added-mass and circulatory contributions, flow separation, vortex roll-up and shedding vary. Both the mean and fluctuating parts of the lift and moment are expected to depend on these parameters. The main objective of this study is to measure the unsteady lift and pitching moment in order to investigate the mean, amplitude and phase of the lift and moment in a wide range of parameters that are relevant to gust encounters and maneuvers of various aircraft.

Secondly, we compare these measurements with the predictions by reduced-order models. The simplest method to predict the variation of lift coefficient for harmonic vertical plunging motion is the Theodorsen theory [8]. The model is based on the attached potential flow assumption and is valid for small amplitude oscillations. Note that the wake is assumed to remain planar. To take into account flow separation and the leading-edge vortex (LEV), one approach is to use empirical modeling like the Leishman-Beddoes model [9]. An alternative reduced-order model is the Goman-Khrabrov method [10], in which the state-space representation of aerodynamic forces and moments for unsteady airfoil motion is proposed. Position of the separation location on the pitching airfoil was taken as the internal state-space variable. However, all these models are semi-empirical and require coefficients which make them less robust. More recently new approaches based on discrete vortex methods have been proposed. Ramesh *et al.* [11] uses the Leading Edge Separation Parameter (LESP) to predict the onset of separation from the leading-edge. The LESP-based Discrete Vortex Method (LDVM) has more potential to quantify the suction effect of coherent vortical structures with a computational cost higher than semi-empirical methods but still significantly lower than the Computational Fluid Dynamics (CFD) methods. In this paper, we will compare these reduced-order models against our experimental data for a plunging airfoil.

In this paper unsteady lift, pitching moment and flow field measurements are performed for a NACA 0012 airfoil undergoing pure-plunging motion with a range of geometrical angles of attack that span pre-stall and post-stall regimes at a low Reynolds number (*Re* = 20,000). These experimental measurements are used to improve understanding of the effect of the vortical flows on the unsteady lift and moment, and as test cases to examine the accuracy of reduced order models including: the Theodorsen, Leishman-Beddoes, Goman-Khrabrov, and the LDVM. The range of amplitudes (*A/c* ≤ 0.5), reduced frequencies (*k* ≤ 1.1) and geometric angles of attack (α=0°, 5°, 9°,

15°, 20°) covers the gust encounter and extreme maneuver range of civil aircraft and micro air vehicles.

II. Methods and Techniques

Unsteady lift, pitching moment and phase-averaged PIV measurements were conducted at *Re* = 20,000 for a NACA0012 airfoil plunging with sinusoidal motion normal to the freestream flow direction, see Figure 1. Five different geometric angles of attack were tested, i.e., α=0°, 5°, 9°, 15° and 20°. These were selected to be representative of the symmetry (0°), pre-stall (5°), stall (9°) and post-stall cases (15° and 20°). The sinusoidal plunging motion has a range of reduced frequency k from 0.0 to 1.1 (St_c=0.35) with peak-to-peak amplitudes of A/c = 0.05, 0.1, 0.3, 0.5. Four reduced-order models (the Theodorsen, Leishman-Beddoes, Goman-Khrabrov, and the LDVM) are compared with the experimental lift/moment data.

A. Experimental setup

The experiments were performed in the closed-loop free surface water tunnel facility at the University of Bath. The water tunnel has a glass working section with dimensions 381 x 508 x 1530 mm. The flow speed range is from 0 to 0.5 m/s with a turbulence intensity of less than 0.5% [12]. The wing is vertically mounted in the working section and attached to a linear motion mechanism, see Figure 2. The wing has a NACA0012 profile with a chord of 62.7 mm and an aspect ratio of 5. It is manufactured through selective laser sintering (SLS) with a polished smooth surface. Inside the wing a 25x5 mm rectangular bar of T800 carbon fibre is inserted to ensure high spanwise stiffness. In order to prevent the tip vortices and spanwise flow, a small carbon fibre plate is attached to the root of the wing, and a fixed aluminum plate is placed 1 mm above the carbon fibre plate. This design minimizes the total mass of the oscillating components in order to keep the wing inertia force small. The oscillating carbon fibre plate extends 0.15c upstream of the wing leading-edge, 0.15c downstream of the trailing-edge and +/-0.8c in the cross-stream direction. The fixed root-plate as well as the glass wing-tip end plate extend 2c upstream, 10c downstream and the full width of the water tunnel in the cross-stream direction.

The wing is connected to a moving carriage through a rotation stage which allows variation of the geometric angle of attack with an accuracy of ±0.2°. The moving carriage is held by four air-bearings that absorb the bending and torque loads whilst enabling frictionless motion. The

plunging motion is supplied by a Zaber LSQ150B-T3 translation stage powered by a stepper motor with an X-MCB1 controller. The plunging motion follows a sinusoidal function with an accuracy of 2%:

$$h = a \cos(2\pi ft) = A/2 \; \cos(2\pi ft) \qquad (2)$$

B. Force and moment measurements

The force measurement system is used to acquire lift and pitching moment in both static and dynamic conditions. A load cell (Futek S-beam tension/compression) is placed between the moving carriage and the motorized translation stage (Figure 2) to measure lift inline with the plunging direction, i.e. normal to the freestream flow direction. By removing the moments, streamwise and spanwise forces through the air bearings it is possible to use a sensitive force sensor to measure the cross-stream force component. A pitching moment sensor (Futek reaction torque sensor) is placed between the moving platform and the wing to measure the pitching moment at the wing ¼ chord. The moving carriage also includes an accelerometer (Strainsense 4807A) which is used to remove inertia forces. To remove this component, the structural mass and inertial moment were multiplied by the instantaneous acceleration during the plunging motion. The calculated inertia force and moment are then subtracted from the raw signal to calculate the net loads.

The static measurements are acquired for 60 seconds at data acquisition rate of 1 kHz. For dynamic measurements, the data acquisition rate is 2,000 times the plunging frequency. From the dynamic measurements the time-average, first harmonic amplitude and phase lag of the lift and moment signals are extracted:

$$C_l(t) \approx a_0 + a_1 \cos(2\pi ft + \phi) \qquad (3)$$
$$C_m(t) \approx b_0 + b_1 \cos(2\pi ft + \beta) \qquad (4)$$

The averages a_0 and b_0 are simply the time-averaged lift and moment. The coefficients a_1 and b_1 represent the amplitudes of the plunging frequency component of the Fourier Transform. The phase lags Φ and β are the corresponding phase differences between the first harmonic of the lift and moment signal and the plunging motion signal. In addition, the phase-averaged lift and

moment are calculated through averaging of 50 periods. The uncertainty in the measurement of lift coefficient C_l is estimated to be ±0.05 for static measurements and ±0.10 for dynamic measurements. The uncertainty in the measurement of pitching moment coefficient C_m is estimated to be ±0.01.

C. Particle Image Velocimetry measurements

Two-dimensional Particle Image Velocimetry (PIV) measurements are taken in a cross-section in the central spanwise plane of the wing, as shown in Figure 2b. The water tunnel was seeded with hollow glass particle with size of 8-12 µm. These particles are illuminated by a New Wave Solo Nd:YAG 50 mJ pulsed PIV laser positioned to the side of the working section. The images are captured through a twelve-bit 4 megapixel charge-coupled device camera positioned below.

Phase-averaged flow field measurements of the velocity field were acquired at intervals of $0.25T$ with averaging over 100 pairs. The wing position was measured through a Renishaw optical linear encoder with an accuracy of 5 µm. The camera was focused on a region from $0.3c$ upstream of the leading-edge to $0.8c$ downstream of the trailing-edge. The images were processed using the software Insight 4G with an interrogation window of 48x48 pixels and a grid overlap of 0.25 giving a spatial resolution of approximately $0.01c$.

D. Reduced-order models

The Theodorsen model identifies two components of the unsteady lift, circulatory and added-mass. The circulatory component can be considered as the quasi-steady component and also includes the effect of wake vorticity. The model can estimate both lift and pitching moment without any empirical coefficients. The Theodorsen formula to estimate the lift coefficient for harmonic vertical plunging motion, $h(t) = ae^{j2\pi ft}$, is given as:

$$C_l = [2\pi kjC(k) - \pi k^2]\frac{A}{c}e^{j2\pi ft} + 2\pi\alpha \qquad (5)$$

The mean lift coefficient is $2\pi\alpha$, which is the same as the thin airfoil prediction for steady flow. The harmonic term contains the circulatory part $2\pi kjC(k)$, which is dominant for low reduced

frequencies, and the added-mass part πk^2, which becomes dominant at high reduced frequencies. The Theodorsen's function $C(k)$ is a complex number that reflects the effects of the shed wake. Its module starts from unity for $k = 0$ and monotonically converges to 0.5 for $k \rightarrow \infty$. In contrast with lift, unsteady pitching moment about the quarter-chord depends only on the added mass effect, with no effect from the circulatory part [13]:

$$C_{m,1/4} = \left[\frac{\pi}{4}k^2\right]\frac{A}{c}e^{j2\pi ft} \qquad (6)$$

For the Leishman-Beddoes model, good agreement with experimental data was reported [9] for airfoil pitching oscillations around the stall angle for reduced frequencies around $k = 0.1$. The semi-empirical model of Leishman-Beddoes gives the unsteady lift as the sum of three different contributions: (i) lift of attached flow, which is a superposition of the circulatory and non-circulatory components; (ii) lift of separated flow, which accounts for trailing-edge separation, and (iii) lift of LEV. The Leishman-Beddoes method (LB) then uses the superposition of indicial responses and the force equations are manipulated as a finite difference approximation of the Duhamel's integral. The movement of the instantaneous separation point is modelled semi-empirically. There are four main time constants that take into account the response of unsteady boundary layers, dissipation time of the LEV, and its convection speed. To ensure an accurate choice of time constant despite the differences in the Reynolds number and the airfoil motion (pitching versus plunging), typical values of the time constants used by Leishman and Beddoes [9] were varied in the range 50% to 200% . No significant improvement was observed. The values chosen, which demonstrated the best agreement with the experimental data, were therefore close to those used by Leishman and Beddoes (using the same notation as Leishman and Beddoes): T_p=1.7, T_f=6.0, T_v=5.0, and T_{vl}=5.0.

In the Goman-Khrabrov method [10], aerodynamic forces can be calculated from a first-order ordinary differential equation and only two empirical constants are needed, which take into account of the response of the separated flows. A slightly modified version of this model was successfully applied to a pitching wing [14]. There are two main constants (time delay and relaxation time constant) that represent the quasi-steady aerodynamic effects and the transient

response of the separated flows. Again, considering the differences in the Reynolds number and the airfoil motion (pitching versus plunging), the values of the time constants used by Goman and Khrabrov have been varied in 50% to 200% range in our calculations. However, we have not observed any improvement and therefore set the same time constants as, $\tau_1 = 0.5c/U_\infty$ and $\tau_2 = 4.5c/U_\infty$ to give the best agreement with the experimental data.

The only semi-empirical constant used in the LDVM method is the critical leading-edge suction parameter, $\text{LESP}_{\text{crit}}$, which depends on the airfoil shape and the Reynolds number. In this approach it is assumed that the roll up of the LEV starts when LESP exceeds the critical value $\text{LESP}_{\text{crit}}$. This prediction is combined with a discrete vortex method to determine the onset, growth and convection of the LEV. In this study, the parameter is set as $\text{LESP}_{\text{crit}} = 0.25$ [15] and we used the same methods described in [11]. We also varied the $\text{LESP}_{\text{crit}}$ parameter in the range of 0.15 and 0.35 to explore the effect of this parameter. However, these did not lead to improved predictions.

III. Results

A. Stationary airfoil

The time-averaged lift for the stationary airfoil is presented in Figure 3. In order to validate the measurement techniques, the time-averaged lift measurements are compared with measurements from the literature. There is a good agreement between the present study with previous measurements from Cleaver *et al.* [16] which used the same water tunnel facility but with a different force measurement system. There is also a reasonable agreement with literature data from other facilities for similar Reynolds numbers [17-19].

At low values of angle of attack both the present measurements and literature [16, 18] exhibit a non-linearity in the form of a reduced slope in the range α<3°. This behavior is related to the effect of airfoil leading-edge curvature at low Reynolds numbers. This characteristic has been observed [20, 21] for a NACA0012 but not for a plate with small camber. It is evident for *Re* < 30,000 and disappears for *Re* higher than 70,000 [21]. Moreover, this effect is not observed if the NACA0012 is reversed.

At higher values of angle of attack some difference is observed in terms of the maximum lift and the value of the stall angle. The wide spread of behavior observed in the literature suggests that static stall and post-stall conditions have a substantial facility dependence. Neverthless, the

current measurements are within the spread observed in the literature. Based on Figure 3, the geometric angles of attack selected for dynamic measurements can be classified as symmetry (0°), pre-stall (5°), stall (9°) and post-stall cases (15° and 20°).

B. Effect of LEV on lift and moment

With increasing mean angle of attack, frequency and amplitude of the oscillations, the flow over the airfoil changes from fully attached to fully separated. Figure 4 shows the effect of the mean angle of attack for the largest frequency and amplitude ($k = 0.94$ and $A/c = 0.5$). For the zero mean angle of attack ($\alpha=0°$), there is a small region of increased clockwise vorticity but nothing that can be described as a coherent LEV. For this extreme condition, there is only mild separation for $\alpha=0°$. For $\alpha \geq 5°$ there is a clear, coherent upper-surface LEV and counter-clockwise secondary vorticity on the airfoil surface. With increasing angle of attack this LEV progressively shifts away from the upper-surface and shifts downstream. Hence, the geometric angle of attack has substantial impact both on the intensity of the LEV and its convection.

Figure 5 compares the lowest and highest mean angles of attack from Figure 4 ($\alpha = 0°$ and $\alpha = 15°$). These will be discussed in terms of the phase-averaged lift and moment to contrast attached flows with those that are dominated by the LEV.

The top row of Figure 5 compares the phase-averaged lift coefficient as a function of the effective angle of attack for $\alpha = 0°$ (left column) and $\alpha = 15°$ (right column) for the same frequency and amplitude: $k=0.94$ and $A/c=0.5$. For comparison, the estimated lift coefficient due to the added-mass of a flat-plate is also included. In the columns below are contour plots of the phase-averaged velocity magnitude for four phases denoted by A, B, C and D (see also Figure 1) in the lift coefficient loops. At the top of the plunging motion, phase A, the flow is substantially attached for both angles of attack. During the downward motion, phase B, the $\alpha = 0°$ case shows no sign of a LEV, whereas the post-stall case ($\alpha = 15°$) shows the roll-up of a strong coherent LEV away from the surface. Around this phase the lift reaches its peak value, while the added-mass contribution is null. Hence, the maximum lift is primarily determined by the circulatory forces for both cases when the effective angle of attack is near the maximum. At the bottom of the motion, phase C, the LEV propagates downstream for $\alpha = 15°$. For the $\alpha = 0°$ case, there is only a mild separation. For both cases the lift is now decreasing. In the middle of the upward motion, phase D (when the effective angle of attack is minimum), the lift coefficient is approximately minimum for both cases.

The shapes of both lift loops are surprisingly similar despite the differences in the vortical flows. In summary, for this high-amplitude high-frequency case, the circulatory lift determines the maximum lift, which is reached near the maximum effective angle of attack, regardless of the effect of the LEV.

Figure 6 illustrates the phase-averaged loop of the pitching moment as a function of the effective angle of attack as well as the vorticity contours for the same plunging conditions as in Figure 5. The effect of the LEV on pitching moment coefficient is more evident. In the case of $\alpha = 0°$ (Figure 6, left), the flow is mostly attached and the pitching moment loop follows the added-mass contribution with generally good agreement. Conversely, for the post-stall angle of attack $\alpha = 15°$, there is significant discrepancy between the experimental measurement and added-mass prediction. The vorticity contour plots clearly show that this difference is due to the formation and convection of the LEV. At the top of the motion, phase A, the flow is primarily attached resulting in the added-mass prediction and experimental measurements being almost coincident. During the downward motion, at phase B, the LEV rolls-up and the difference between measurements and added-mass prediction increases. At the bottom of the motion, at phase C, the pitching moment is slightly negative ("nose-down"), which is in stark contrast with the added-mass prediction of "nose-up" moment. This can be attributed to the suction effect of the convecting LEV producing a negative pitching moment around the ¼c. In other words, the positive pitching moment produced by the added-mass effect is compensated by the negative moment produced by the suction of the LEV. As the LEV convects downstream past the trailing edge at phase D, the negative pitching moment moves closer to the added-mass loop. It is clear that the LEV strongly influences the pitching moment behavior. In summary, for mostly attached flows the pitching moment is determined by the added-mass effect, whereas the LEVs strongly influence the moment for separated flows. In the following sections, unsteady lift and moment are discussed as a function of reduced frequency and amplitude for the entire range of the test matrix.

C. Unsteady lift

This section analyzes the mean, first harmonic amplitude and phase of lift coefficient. These quantities are compared with the predictions of the reduced-order models. In Figure 7, measured time-average lift coefficient (solid symbols) is compared with the predictions from the Theodorsen theory and the LDVM method (left column), and the semi-empirical methods Leishman-Beddoes

(LB) and Goman-Khrabrov (GK) (right column), for four amplitudes A/c=0.05, 0.1, 0.3 and 0.5 as a function of reduced frequency k. For $\alpha \leq 9°$, the measured mean lift coefficient is reasonably constant across the entire frequency range for the two lowest amplitudes, however the two largest amplitudes demonstrate an increase at high reduced frequencies. The mean value from the Theodorsen theory has a constant value of $2\pi\alpha$, with no dependence on the reduced frequency and therefore does not capture this behaviour. However, the LDVM method provides good prediction of mean lift with increasing frequency and amplitude, up to the stall angle of attack α=9° (Figure 7, left). For these pre-stall and stall angles of attack, the LB and GK methods do not capture the behavior well (Figure 7, right).

For the post-stall cases, α=15° and 20°, the agreement between the experiments and reduced order models is poor. The experiments show a clear increase in mean lift with the gradient being clearly amplitude dependent. Similar behavior was also observed in Cleaver *et al.* [22] for a much larger range of reduced frequency and attributed to the LEV. These previous measurements are also shown for α=15°. The agreement with the current measurements is within the bounds of experimental uncertainty. The LDVM, LB and GK methods all predict an increase but do not capture the qualitative or quantitive behavior. In the case of LDVM the agreement is reasonable only for high reduced frequency $k > 0.6$ and high amplitude $A/c \geq 0.3$. The disagreement at lower amplitudes and frequencies may be related to the LDVM not representing trailing-edge separation [11]. Although the LDVM is better than the other reduced-order models in general, the difference between the experiments and the LDVM is significant for low frequencies and amplitudes. The mean lift predictions from the semi-empirical LB and GK provide reasonable prediction only for low reduced frequencies, and lose accuracy for $k \geq 0.6$. The LB indicial formulation appears to be better in predicting the trend than the state-space formulation proposed by Goman-Khrabrov [10]. However, the relative success of these two methods at low reduced frequencies stems from the fact that the modelling is based on the static airfoil case, and uses the experimentally measured lift for $k = 0$.

The mean-lift enhancement is well known for periodically plunging airfoils at the post-stall angles of attack (see for example, Cleaver et al. [22]. It is clear from Figure 7 that the mean-lift enhancement is also possible at the pre-stall angles of attack with increasing frequency and amplitude, since these conditions will cause LEV formation and shedding. The "vortex lift" has also been observed in other unsteady flows, including the periodic oscillations of freestream

magnitude [23, 24] and the surging motion of airfoils [25]. The mean lift enhancement is expected to depend on the strength of the LEVs (hence St_A) as well as the time spent by the LEVs over the airfoil (hence St_c or k). Other phenomenon such as the resonance with the natural vortex shedding in the wake (typically at high k values, $k > 1.5$) depends on the Strouhal number based on the chord length, St_c (or k) [7, 22]. For the conditions in the present experiments ($k \leq 1.1$ and $St_A \leq 0.18$), there is an indication that St_A may be the dominant parameter. For example, Cleaver *et al.* [22] showed that in the range of $0 \leq St_A \leq 0.3$ for a single angle of attack of $\alpha = 15°$, there is a very good collapse of the mean-lift data when plotted as a function of St_A. The present data covers a wide range of angles of attack, including both the pre-stall and post-stall incidences. Figure 8(a) shows the variation of the difference between the mean-lift coefficient and the static-lift coefficient, ($C_{l,mean} - C_{l,static}$), as a function of St_A for all angles of attack. Although there is a collapse across different amplitudes for a single angle of attack, there is not a collapse of the data across different angles of attack. Figure 8(b) presents the variation of ($C_{l,mean} - C_{l,static}$) as a function of the maximum effective angle of attack, which combines the geometric angle of attack and St_A by definition. Interestingly, there seems to be a better correlation for the whole data set. No substantial lift enhancement is observed until around 15°. For $\alpha_{eff,max} \geq 15°$, there is a trend of a linear relationship between $\alpha_{eff,max}$ and lift enhancement.

In Figure 9, the amplitude of the unsteady lift as a function of k is shown and compared with the predictions of the reduced-order models. For the pre-stall geometric angle of attack, $\alpha \leq 5°$, there is excellent agreement between the Theodorsen predictions and experimental measurements. This is surprising given the large amplitudes of oscillations that invalidate the planar wake assumption and large effective angles of attack, up to 45°, that invalidate the attached flow assumption. In fact, for $\alpha = 5°$, the formation of a LEV at the high frequency and amplitude was already shown in Figure 4. The variation of the lift amplitude is approximately parabolic, consistent with Equation (5). While the predictions of the LDVM is also good for $\alpha \leq 5°$, the LB and GK models only capture the trend, but with poor agreement with the experiments.

For the stall and post-stall cases, the experimental data show deviations from the nearly parabolic variation, with an inflection point or a local peak in the range of $0.4 \leq k \leq 0.8$. With increasing angle these peaks become more pronounced. The Theodorsen's method predicts the general trend but not the peaks, the LDVM however does predict the peaks reasonably well. This would suggest that the peaks are related to the vortex dynamics. The LB semi-empirical method

provides reasonable predictions of the lift amplitude (Figure 9, right), however, it is not as good as the Theodorsen predictions. On the other hand, the GK method tends to over-estimate the lift amplitude (Figure 9, right), in particular for high plunging reduced frequencies. It also tends to predict the peaks observed at higher angles of attack, but only qualitatively.

It was unexpected that the predictions of the Theodorsen theory vary from excellent to reasonable as the angle of attack is increased from the pre-stall regime to the post-stall regime. While separated and vortical flows are present at high frequencies and amplitudes even for pre-stall angles of attack, the agreement with the theory is very good, and becomes still reasonable at post-stall angles of attack. The added-mass contribution and the circulatory contribution, which was originally developed for attached flows and includes the wake effect of shed vorticity, are able to predict the lift amplitude successfully. On the other hand, it should be kept in mind, none of the reduced-order models were able to predict the mean lift. The relative success of the models for the lift amplitude, but not for the mean lift, is intriguing. In comparison, for airfoil surging motion potential flow models can accurately predict the unsteady lift at pre-stall, but not at post-stall angles of attack [25, 26]. The question of why there are such differences remains unanswered.

For many applications, the maximum lift attained during the cycle is important. As shown in Figure 5 the maximum lift occurs near the maximum effective angle of attack for our range of parameters. Using Equation (3), we plot in Figure 10 the maximum lift coefficient $C_{l,max}$ as a function of the maximum effective angle of attack, $\alpha_{eff,max}$ for all cases. Also included is the lift calculated through the linear theory: $2\pi\alpha_{eff,max}$. It is noteworthy that the data points are mostly distributed close to or below the linear theory. The points with largest deviations from the linear trend are those for higher angles of attack with low Sr_A, *i.e.*, static or near static cases with $k\rightarrow0$. Overall, it is very interesting that the plunging motion with separated flows result in a maximum lift that is equivalent to what is predicted by the attached flows. This can be used as a conservative estimate for the maximum lift during a gust or maneuver.

The phase lag of the lift with respect to the plunging motion is shown in Figure 11 alongside the two more promising reduced-order model (the Theodorsen and the LDVM) predictions. Overall, except for small reduced frequencies the Theodorsen theory provides reasonable prediction for the majority of plunging conditions. For pre-stall angles of attack the region of small reduced frequencies where there is deviation from the experiments is small. It is worth noting that although the measurement uncertainty for the phase lag estimation increases in this region, it is

also the region in which the circulatory contribution to the lift is dominant. Therefore, flow separation, in particular the trailing-edge separation, might contribute to this behavior. With increasing frequency, the added-mass contribution increases, which results in better agreement between the Theodorsen theory and the experiments, even though separated and vortical flows become dominant. This is in agreement with the findings for a flat plate at similar conditions, despite the existence of leading-edge separation [27]. The disagreement between the experiments and the Theodorsen theory in Figure 11 becomes larger over a wider region for the stall (α=15°) and the post-stall (α=20°) angles of attack. This region at low reduced frequencies is also where the LDVM is not capable of accurate predictions as discussed earlier. Even with increasing reduced frequency, the LDVM does not provide improvement in comparison with the Theodorsen method and is worse for the largest angle of attack α=20°, particularly for low plunging amplitudes $A/c \leq$ 0.1.

As the Theodorsen theory is capable of predicting the amplitude and the phase of the lift even for separated flows, the shape of the loops of lift as a function of effective angle of attack can be successfully predicted if the mean lift is corrected. In Figure 12, the measured phase-averaged lift for different angles of attack at $k = 0.94$ and $A/c = 0.5$ is compared with the Theodorsen prediction, which is shifted to the measured mean lift instead of the theoretical $2\pi\alpha$. For comparison, the added-mass contribution is also shown. Phase-averaged stream-lines with velocity magnitude contours are presented in Figure 12 (right column) for phase B (t/T=0.25, the middle of the downward motion), when the effective angle of attack is maximum. Overall, the measured phase-averaged lift is reasonably close to the corrected Theodorsen prediction for all angles of attack (Figure 12, left). With increasing angle of attack the LEV becomes progressively stronger and the deviations from the corrected Theodorsen prediction increases. Nevertheless, the agreement is generally very good even at the highest angle of attack where the LEV produces an increase of the peak lift of about 10%. Hence, the hysteresis of the lift can be predicted by the corrected Theodorsen theory, even for separated flows. In summary, the total unsteady lift can be estimated reasonably well with the Theodorsen theory, provided a corrected value of mean lift is used. The correlation of the mean lift, presented in Figure 8, can be considered as a first attempt at empirical modeling of the mean lift.

D. Unsteady Pitching Moment

Figure 13 presents the variation of the mean (left) and the amplitude (right) of the pitching moment at ¼ of the chord as a function of plunging reduced frequency and the peak-to-peak amplitude *A/c* at various geometrical angles of attack. In the case of the time-averaged pitching moment, the Theodorsen theory predicts it as zero, since it depends only on the added mass effect (see Equation (6)). Our experimental data for $\alpha = 0°$ are consistent with this prediction. This is because there is no LEV formation for $\alpha = 0°$ as discussed earlier. However, for $\alpha = 5°$ and $\alpha = 9°$, the mean pitching moment becomes negative (nose-down) with increasing frequency and amplitude as LEV shedding becomes more predominant, whereas the mean moment is around zero for $k = 0$. For post-stall angles of attack $\alpha = 15°$ and $20°$, the mean pitching moment is already nonzero and negative at $k = 0$, consistent with the separated flows for the stationary airfoil. With increasing reduced frequency and amplitude, the mean moment generally becomes more negative. It is noteworthy that, for post-stall angles of attack $\alpha = 20°$, at high reduced frequency $k \approx 1.0$, there is even some non-monotonic variation with the amplitude *A/c*. The LDVM predictions of the mean pitching moment capture some of the experimental trends, but not accurately.

The pitching moment amplitude is shown in Figure 13 (right column). For pre-stall angles of attack, the measured amplitude of C_m follows a parabolic trend with *k* as predicted by Equation (6), however it is somewhat smaller than the Theodorsen prediction. We observe that the LDVM predictions do not offer any improvement for pre-stall angles of attack. The trend of the measured C_m amplitude is more complex for stall and post-stall angles of attack. Indeed, for $\alpha \geq 9^0$ the relation between the amplitude of C_m and the plunging reduced frequency *k* is not monotonic, but is characterized by a local maximum and a local minimum in this range of *k* (Figure 13, right column). In this flow regime, roll-up and shedding of the LEVs are the dominant features. For these angles of attack, predictions of the Theodorsen theory are unreliable. Interestingly, the LDVM predictions capture the trend and even locate the range of reduced frequencies at which local maximum are observed. However, magnitude of the peaks is not predicted accurately for higher amplitudes. Generally, the magnitude of C_m is over-estimated by the LDVM.

Depending on the geometric angle of attack, the mean pitching moment at zero frequency may be negative. It appears that with increasing frequency and amplitude, the mean moment becomes more negative due to the LEV formation and shedding. The variation of the difference between the mean pitching moment coefficient and the pitching moment coefficient of the stationary airfoil

16

($C_{m,mean} - C_{m,static}$) is shown in Figure 14 as a function of the maximum effective angle of attack. The choice of the latter parameter was discussed previously in relation to the mean-lift enhancement. Figure 14 shows reasonable collapse of the data, although there is larger scatter in comparison with the mean-lift enhancement (see Figure 8). It is seen that the deviations from the static moment start once $\alpha_{eff,max}$ is larger than 10°. The minimum pitching moment (largest nose-down pitching moment) may be expected to be more complex, given that the amplitude variations shown in Figure 13 are highly non-monotonic. Figure 15 shows the variation of the minimum pitching moment coefficient $C_{m,min}$ as a function of the maximum effective angle of attack. The collapse of the data is still reasonable, although the scatter is larger compared to the maximum lift coefficient (see Figure 10).

In order to understand the effect of the LEVs, the phase-averaged C_m is plotted in Figure 16 for four angles of attack at the same plunging conditions, k=0.94 and A/c=0.5, together with the contour plots of the spanwise vorticity. The added-mass contribution is also included, which is the only term in the Theodorsen prediction (Equation 6). The vorticity contours at the upstroke of the plunging (t/T=0.0, phase A) show no vortex roll-up over the wing for all angles of attack. Indeed, the point A in the phase-averaged C_m is close to the added-mass loop for all cases, and is also approximately the point with the largest nose-down pitching moment. Conversely, at the downstroke of the plunging motion, i.e., t/T=0.5 (phase C), the difference between measured pitching moment and added-mass value increases with the angle of attack as seen in Figure 16. The vorticity contours show that the size of the LEV increases with the geometrical angle of attack α. Moreover, the position of the LEV progressively moves downstream as α is increased. Hence, it is inferred that, at high k and A/c, the pitching moment during the downstroke depends both on the intensity and the position of the LEV. Indeed, a downstream shift of the LEV increases the moment arm of the LEV with respect to ¼ of the chord. The moment produced by the LEV is opposed to the moment of the added-mass effect and therefore the amplitude of C_m variation is reduced with increasing angle of attack which also causes the mean value to decrease (see also Figure 13).

The varying nature of the separated flow and LEV roll-up cause strongly non-monotonic variation of the pitching moment amplitude at post-stall angles of attack (see Figure 13 right column). In order to shed further light on this observation, the phase-averaged C_m is plotted in Figure 17 for two different plunging reduced frequencies at α=15^0 and plunging peak-to-peak

amplitude A/c=0.5. We chose k =0.24 (near local maximum) and k =0.47. At the lowest frequency k=0.24, it is observed that there is a spike of nose-down pitching moment during the downward plunging motion at t/T=0.25 (phase B). The phase-averaged spanwise vorticity in Figure 17 reveals that the LEV is closer to the trailing-edge at phase B, providing a relatively large moment arm and resulting negative moment. As the plunging motion continues, the vortical structure moves downstream of the trailing edge and the pitching moment quickly becomes less negative by phase C. As the plunging airfoil moves upwards, the flow separation reduces (phase D) and the pitching moment becomes closer to the added mass loop. In contrast, at plunging reduced frequency k=0.47 the amplitude of the moment is reduced and the spike in nose-down C_m is not observed. A coherent vortex is observed at phase B, however its moment arm appears to be relatively small, resulting in smaller change in the pitching moment.

IV. Conclusions

Unsteady lift, pitching moment and flow field measurements were presented for a periodically plunging NACA 0012 airfoil at a Reynolds number of 20,000. The ranges of reduced frequency (k ≤ 1.1) and peak-to-peak amplitude (A/c ≤ 0.5) were selected to cover the gust encounter and extreme maneuver range of various aircraft of different size. The variations of the lift and pitching moment were studied as a function of effective angle of attack, which varies during the cycle due to the motion of the airfoil. The measurements were compared with various reduced order models. Both pre-stall and post-stall mean angles of attack were considered. Flow measurements showed that, near the maximum values of the reduced frequency and amplitude, the flow over the airfoil during the cycle varies from nearly attached to vortex-dominated, depending on the mean angle of attack.

Within the range of the parameters the circulatory lift, as opposed to the added-mass, determines the maximum lift in the cycle. This occurs near the maximum effective angle of attack regardless of whether an LEV is formed or not. This maximum lift coefficient in the cycle has an upper boundary of $2\pi\alpha_{eff,max}$. However, the effect of the LEV on the mean lift is generally an increase, which seems better correlated with $2\pi\alpha_{eff,max}$, rather than Strouhal number based on the amplitude St_A. The increase in the time-averaged lift, which cannot be predicted by the Theodorsen theory, is also difficult for other reduced-order models. In contrast, the lift amplitude is predicted well by

the Theodorsen theory, whether an LEV is present or not. Even the phase of the unsteady lift is reasonably predicted, in particular at higher reduced frequencies. As a result, the hysteresis loop of the lift as a function of effective angle of attack can be successfully predicted by the Theodorsen theory if the mean lift is corrected.

The effect of unsteady motion is more complex for the pitching moment about the quarter-chord location, and more dependent on whether LEVs are formed or shed. For nearly attached flows, the pitching moment follows approximately the added-mass contribution as predicted by the Theodorsen theory (the circulatory contribution is zero). The maximum nose-down moment occurs when the airfoil is at the top of the motion. For vortex-dominated flows, large deviations from the added-mass contribution occur. There is generally an increase in the time-averaged nose-down moment, which correlates reasonably with the maximum effective angle of attack of the motion. The maximum nose-down moment in the cycle may occur at different phases, depending on the reduced frequency and consequently on the motion of the LEV over the airfoil. At high reduced frequencies, the added-mass contribution is relatively large, therefore the phase of the maximum nose-down moment occurs when the airfoil is at the top of the motion, while the rest of the moment loop is substantially modified due to the motion of the LEV. At lower reduced frequencies, the effect of LEV becomes dominant as the added-mass effect is smaller, and the phase of the maximum nose-down moment correlates well with the timing of the arrival of the LEV at the trailing-edge. Hence, the amplitude of the pitching moment becomes highly dependent on the reduced frequency. The non-monotonic variation of the moment amplitude becomes a clear feature in the existence of the LEVs. While the Theodorsen theory cannot predict the mean and amplitude of the moment, the LDVM captures the trends but the quality of the agreement is variable.

Acknowledgments

References

[1] Mueller, T. J., and DeLaurier, J. D., "Aerodynamics of Small Vehicles," *Annual Review of Fluid Mechanics*, vol. 35, 2003, pp. 89-111. doi: 10.1146/annurev.fluid.35.101101.161102

[2] Shyy, W., Aono, H., Chimakurthi, S.K., Trizila, P., Kang, C.K., Cesnik, C.E.S., et al., "Recent progress in flapping wing aerodynamics and aeroelasticity." *Progress in Aerospace Sciences*, Vol. 46(7), 2010, pp. 284-327.

[3] Platzer, M.F., Jones, K.D., Young, J., and Lai, J.C.S., "Flapping-Wing Aerodynamics: Progress and Challenges," *AIAA Journal*, Vol. 46, No. 9, 2008, pp. 2136-2149. doi:10.2514/1.29263

[4] McCroskey, W.J., "Unsteady Airfoils", Ann. Rev. Fluid Mech. 1982. 14:285-311

[5] Dowell, E.H. and Hall, K.C., "Modeling of Fluid-Structure Interaction", Annu. Rev. Fluid Mech. 2001. 33:445–490.

[6] Von Karman, TH. And Sears, W.R., "Airfoil Theory for Non-Uniform Motion", Journal of the Aeronautical Sciences, vol. 5, August 1938, number 10, pp. 379-390.

[7] Gursul, I., and Cleaver, D.J. " Plunging Oscillations of Airfoils and Wings: Progress, Opportunities and Challenges." *AIAA Journal*, 2018, Article in Advance. Doi: 10.2514/1.J056655.

[8] Theodorsen, T., "General Theory of Aerodynamic Instability and the Mechanics of Flutter," NACA Technical Report, No. 496, NACA, 1949.

[9] Leishman, G. J., and Beddoes, T. S., "A Semi-Empirical Model for Dynamic Stall," *Journal of the American Helicopter Society*, vol. 34, no. 3, 1989, pp. 3–17.

[10] Goman, M. and Khrabrov, A. "State-Space Representation of Aerodynamic Characteristics of an Aircraft at High Angles of Attack", Journal of Aircraft, Vol. 31, No. 5, Sept.-Oct. 1994, pp. 1109-1115.

[11] Ramesh K., Gopalarathnam, A., Granlund, K., Ol, M. V., Edwards, J. R., "Discrete-Vortex Method with Novel Shedding Criterion for Unsteady Aerofoil Flows with Intermittent Leading-Edge Vortex Shedding", *Journal of Fluid Mechanics*, vol. 751, 2014, pp. 500-538.

[12] Heathcote, S., "Flexible Flapping Airfoil Propulsion at Low Reynolds Numbers," Ph.D. Dissertation, Department of Mechanical Engineering, Univ. of Bath, Bath, England, U.K., 2006.

[13] Leishman, J. G., Principles of Helicopter Aerodynamics, 2nd ed., Cambridge University Press, 2006, chap. 8-9. Page 436.

[14] Williams, D.R., Reißner, F., Greenblatt, D. and Müller-Vahl, H., and Strangfeld, C., "Modeling Lift Hysteresis on Pitching Airfoils with a Modified Goman–Khrabrov Model", AIAA Journal, Vol. 55, No. 2, February 2017, pp. 403-409.

[15] Ramesh K, private communication.

[16] Cleaver, D. J., Wang Z., and Gursul, I., "Vortex Mode Bifurcation and Lift Force of a Plunging Airfoil at Low Reynolds Numbers," 48th AIAA Aerospace Sciences Meeting, Orlando, Florida, AIAA Paper 2010-390, 2010.

[17] Kim, D.-H., Chang, J.-W., and Chung, J., "Low-Reynolds-Number Effect on Aerodynamic Characteristics of a NACA 0012 Airfoil," *Journal of Aircraft*, Vol. 48, 2011, pp. 1212–1215.

[18] Wang, S., Zhou, Y., Alam, M., Yang, H., "Turbulent intensity and Reynolds number effects on an airfoil at low Reynolds numbers", *Physics of Fluids*, Vol. 26, 2014. Doi: 10.1063/1.4901969

[19] Schluter, J. U., "Lift Enhancement at Low Reynolds Numbers Using Self-Activated Movable Flaps," *Journal of Aircraft*, Vol. 47, 2010, pp. 348–351.

[20] Lee T., and Su, Y. Y., "Low Reynolds number airfoil aerodynamic loads determination," *Experiments in Fluids,* vol. 53, 2012, pp. 1177–1190.

[21] Laitone, E. V., "Wind tunnel tests of wings at Reynolds numbers below 70 000," *Experiments in Fluids,* vol. 23, 1997, pp. 405-409.

[22] Cleaver, D. J., Wang, Z., Gursul, I., and Visbal, M. R., "Lift Enhancement by Means of Small-Amplitude Airfoil," *AIAA Journal*, vol. 49, no. 9, 2011, pp. 2018-2033. doi: http://dx.doi.org/10.2514/1.J051014

[23] Gursul, I., and Ho, C.M., "High Aerodynamic Loads on an Airfoil Submerged in an Unsteady Stream," *AIAA Journal*, Vol. 30, No. 4, 1992, pp. 1117-1119.

[24] Gursul, I., Lin, H., and Ho, C.M., "Effects of Time Scales on Lift of Airfoils in an Unsteady Stream," *AIAA Journal*, Vol. 32, No. 4, 1994, pp. 797-801.

[26] Granlund, K., Monnier, B., Ol, M., and Williams, D., "Airfoil Longitudinal Gust Response in Separated vs. Attached Flows," *Physics of Fluids*, Vol. 26, No. 2, 2014, p. 027103.

[25] Choi, J., Colonius, T., and Williams, D.R., "Surging and Plunging Oscillations of an Airfoil at Low Reynolds Number," *Journal of Fluid Mechanics*, Vol. 763, 2014, pp. 237-253. doi:10.1017/jfm.2014.674

[27] Son, O. and O. Cetiner. "Force-motion phase relations and aerodynamic performance of a plunging plate." *Experiments in Fluids,* Vol. 59(2), 2018, pp. 28.
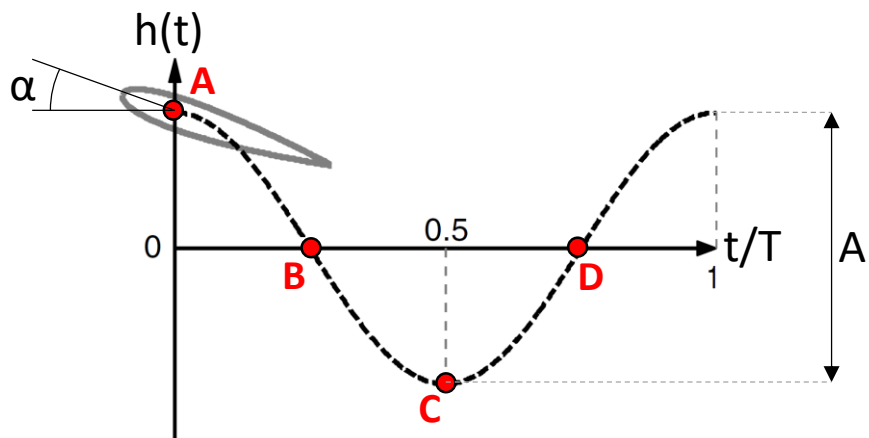
Figure 1. Definition of plunging motion.

a)

FREESTREAM
FLOW

b)

Lift
Sensor

Torque
Sensor

Laser
Sheet

CAMERA
POSITION
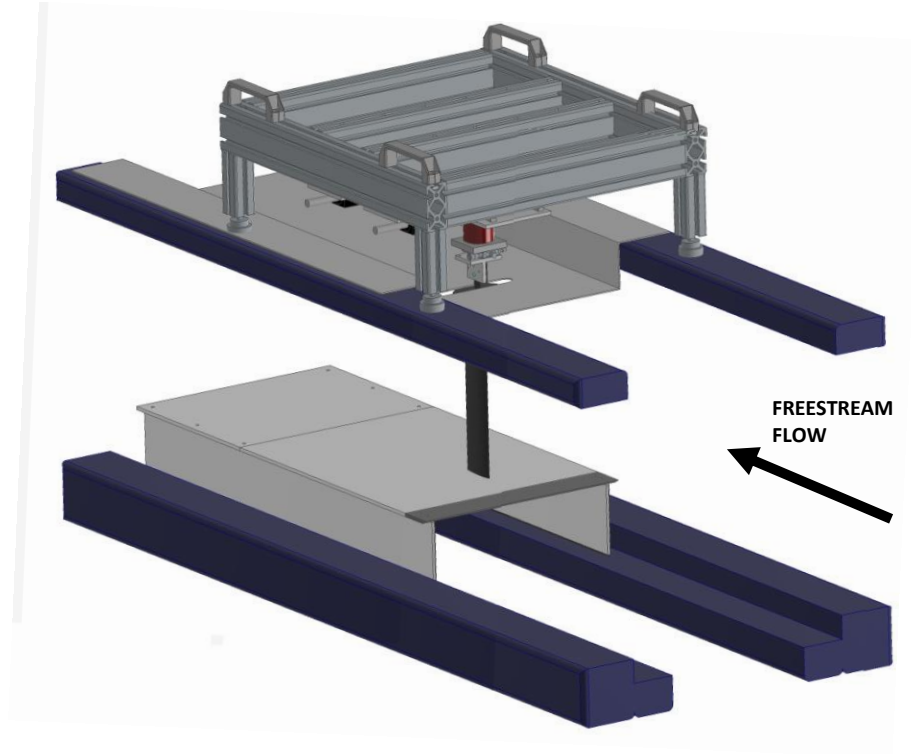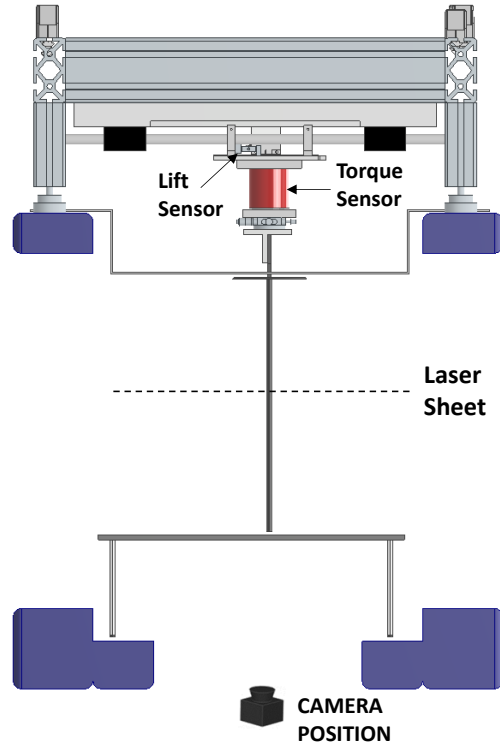
Figure 2. Experimental setup, a) isometric view and b) front view.

23
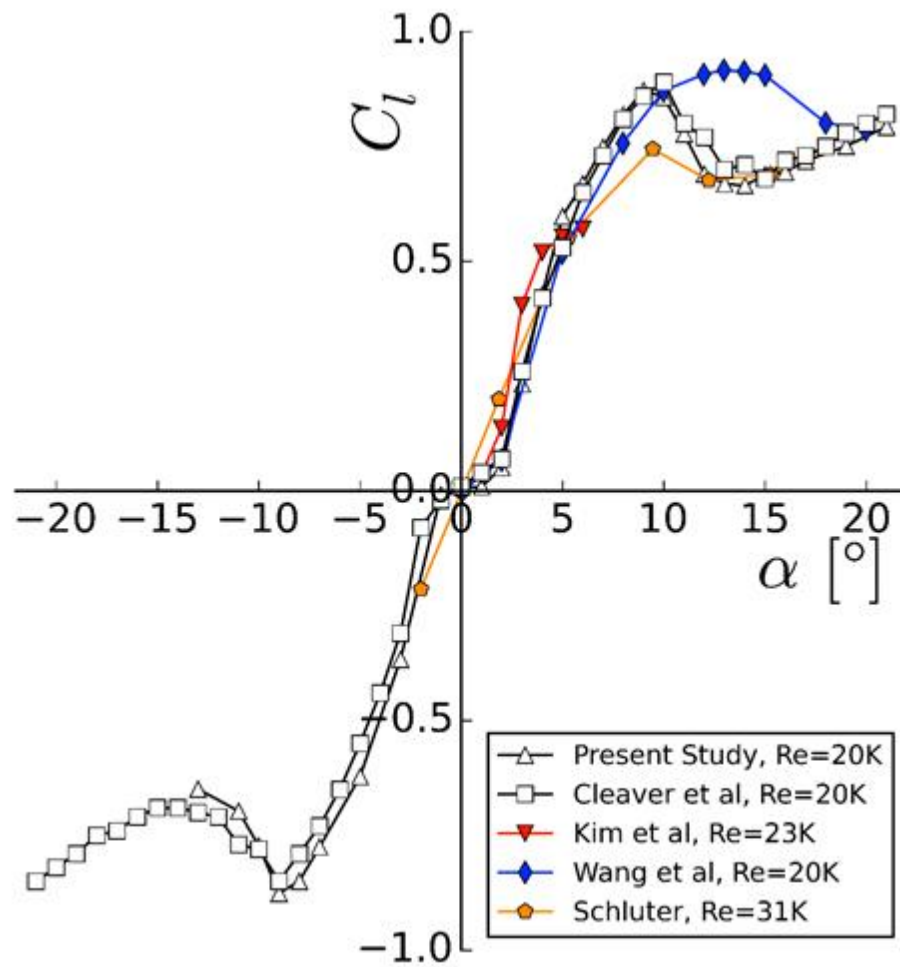
Figure 3. **Variation of lift coefficient with angle of attack for stationary airfoil and comparison with literature data.**
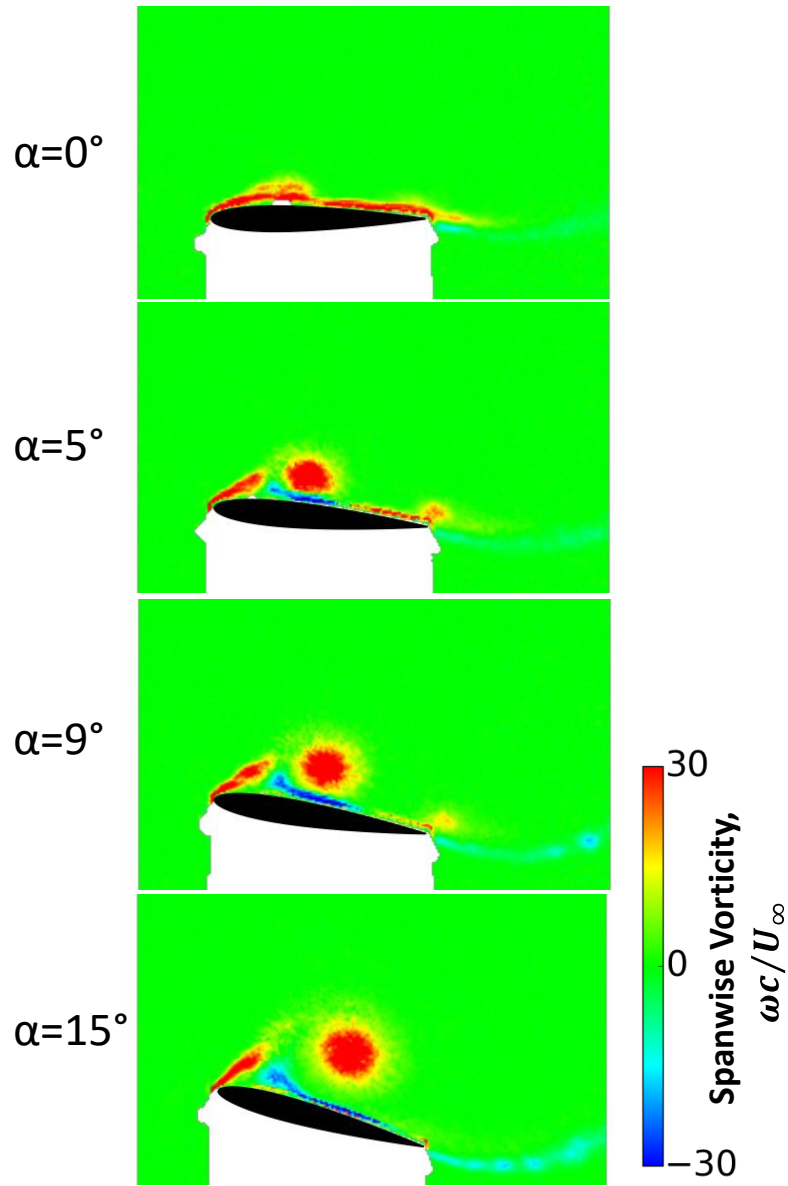
Figure 4. Phase-averaged vorticity for plunging reduced frequency of k**=0.94 and peak-to-peak amplitude** A/c**=0.5 at phase** t/T**=0.5 for** α**=0°, 5°, 9°, and** α**=15°.**
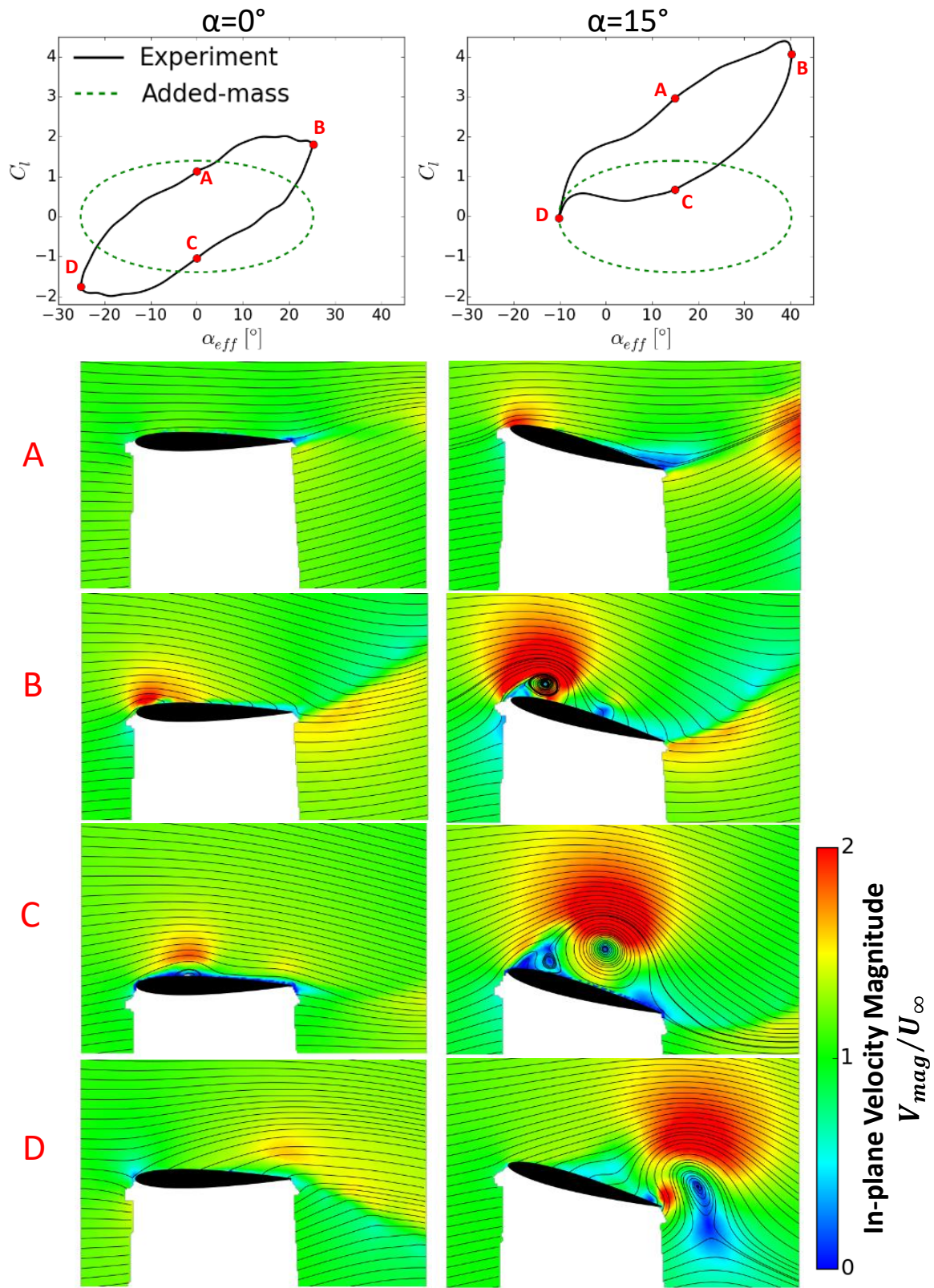
Figure 5. Phase-averaged lift coefficient, velocity magnitude and streamlines for plunging reduced frequency of *k*=0.94 and peak-to-peak amplitude *A/c*=0.5 for α=0° and α=15°.
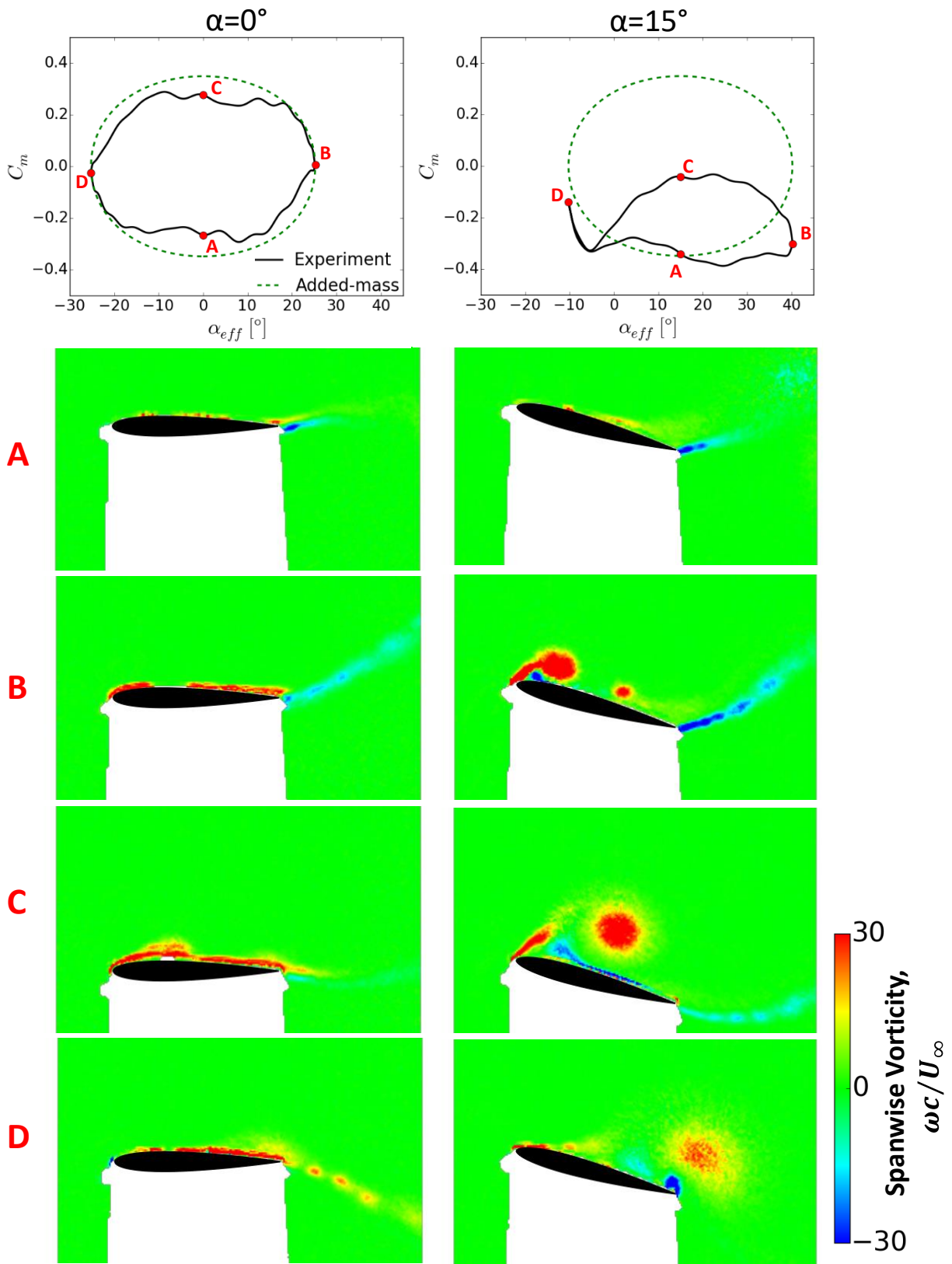
Figure 6. Phase-averaged pitching moment coefficient and vorticity for plunging reduced frequency of k=0.94 and peak-to-peak amplitude A/c=0.5 for α=0° and α=15°.
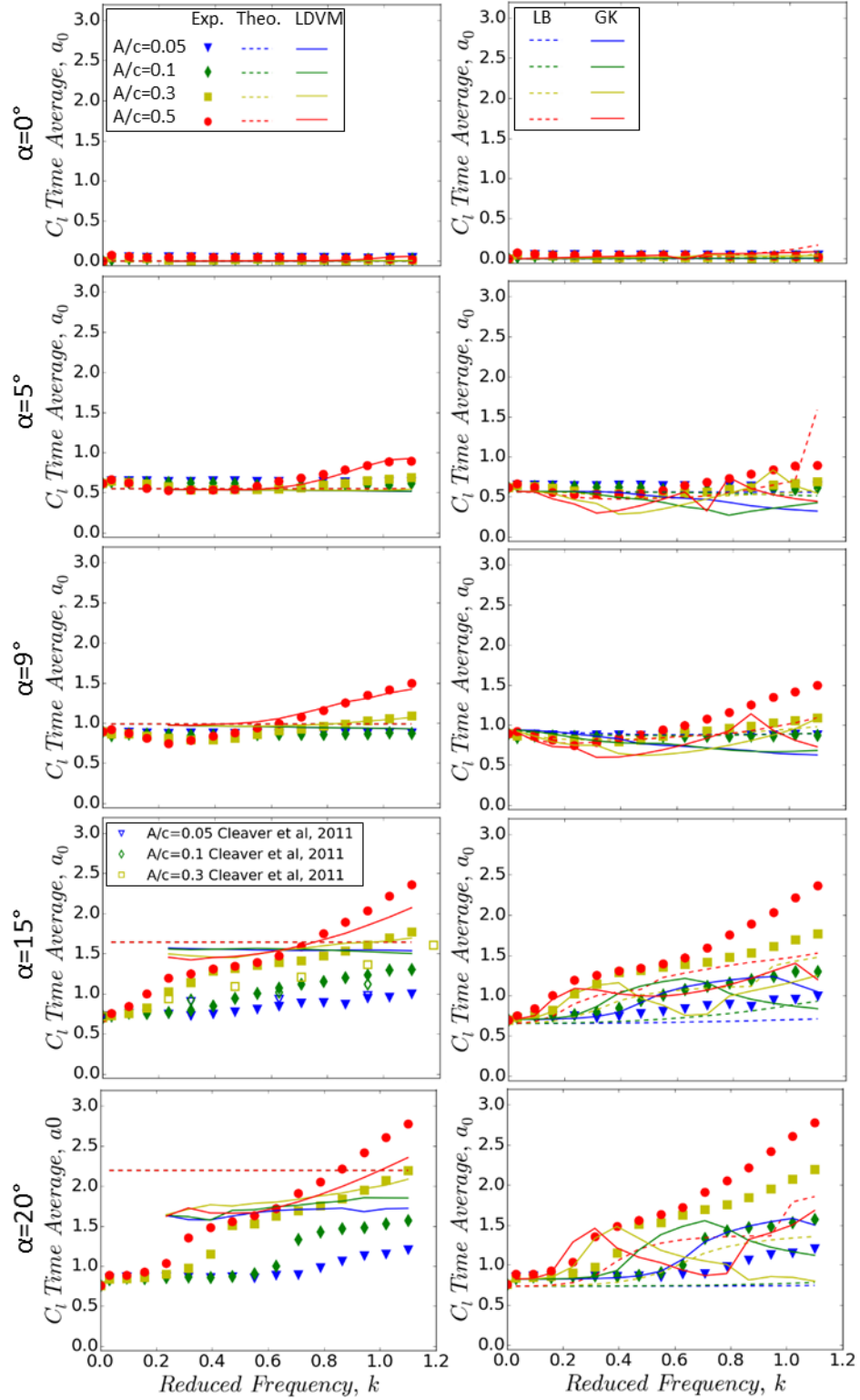
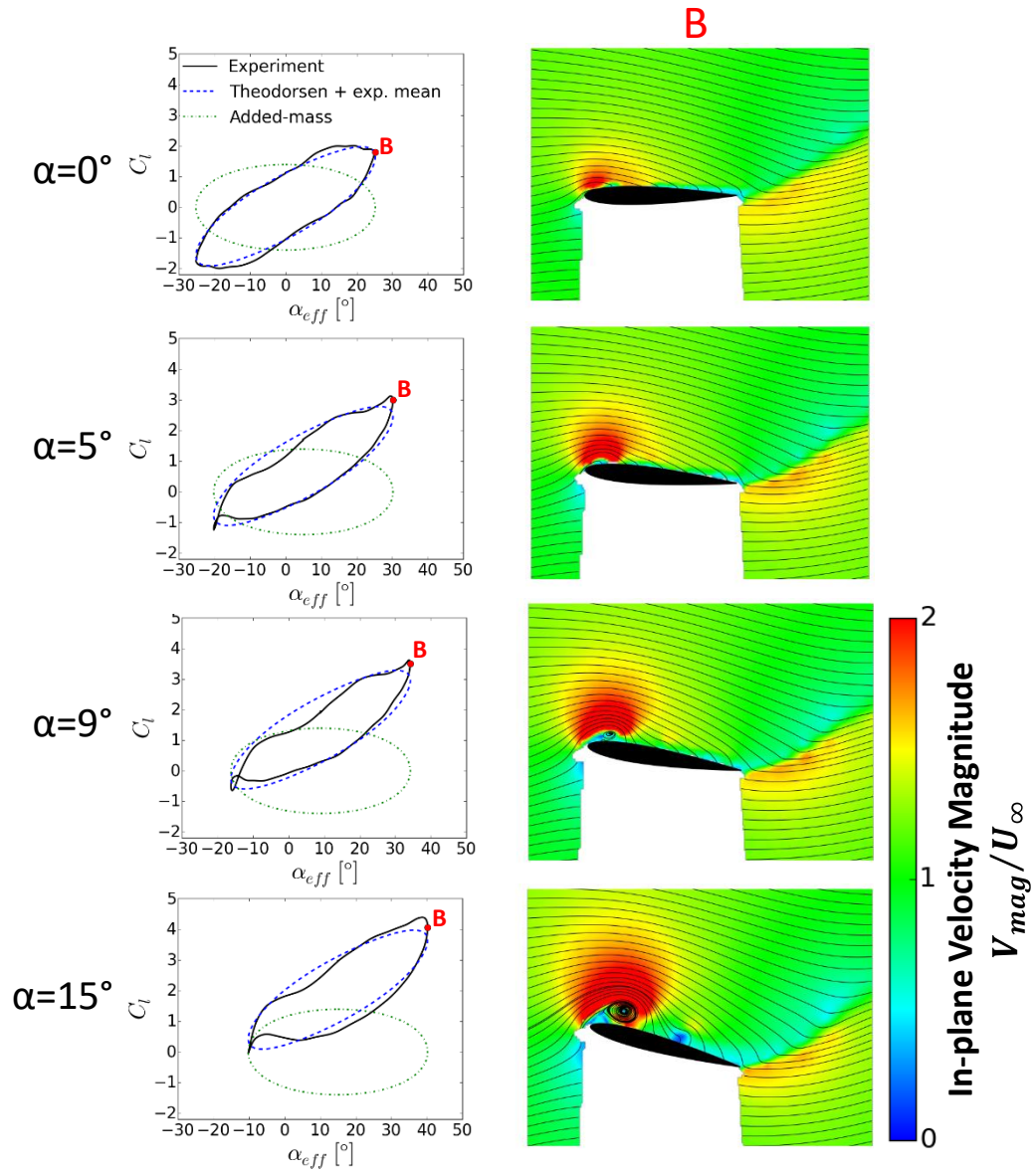**Figure 7. Time-averaged lift coefficient as a function of plunging reduced frequency *k* and amplitude *A/c*, and comparison with Theodorsen and LDVM methods (left), and LB and GK methods (right).**
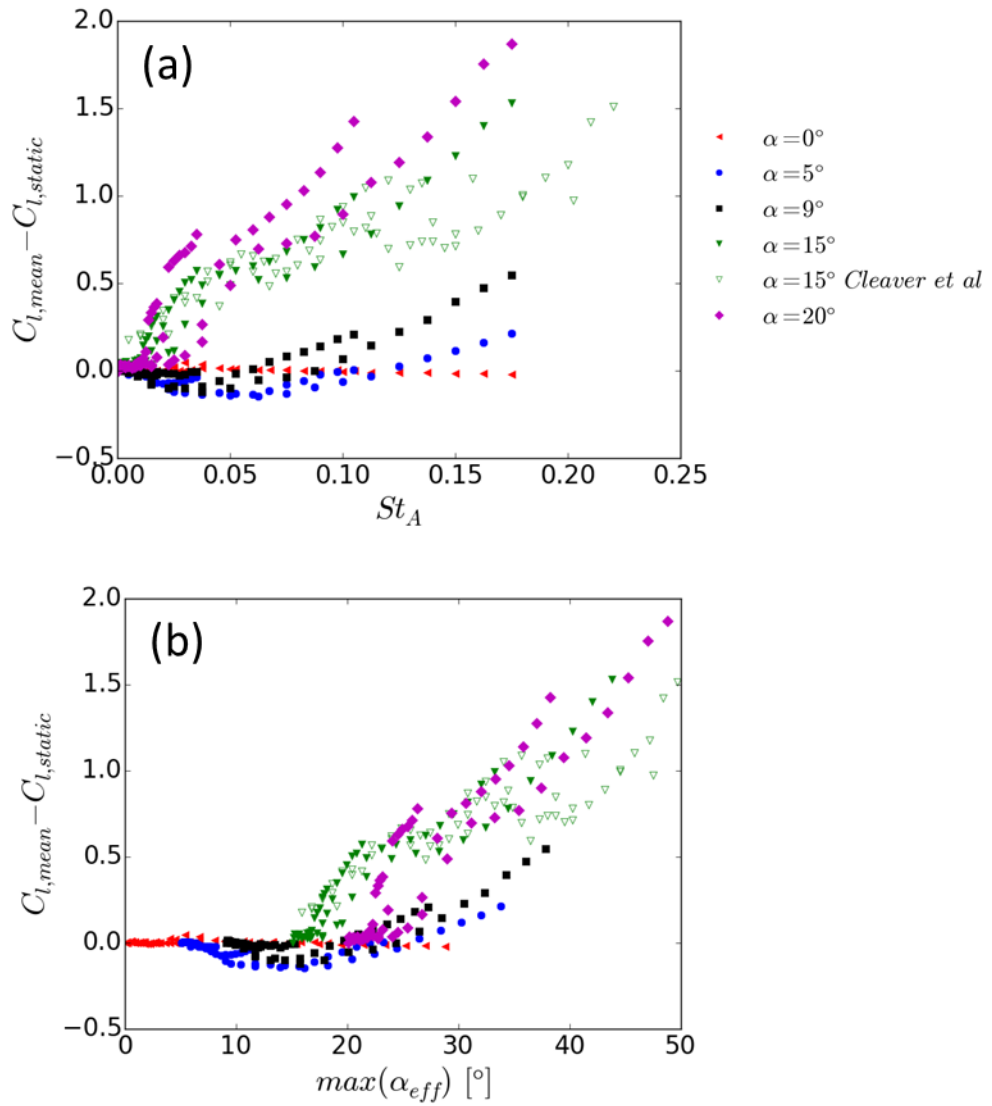
Figure 8. Variation of mean-lift enhancement as a function of (a) St_A, and (b) maximum effective angle of attack.
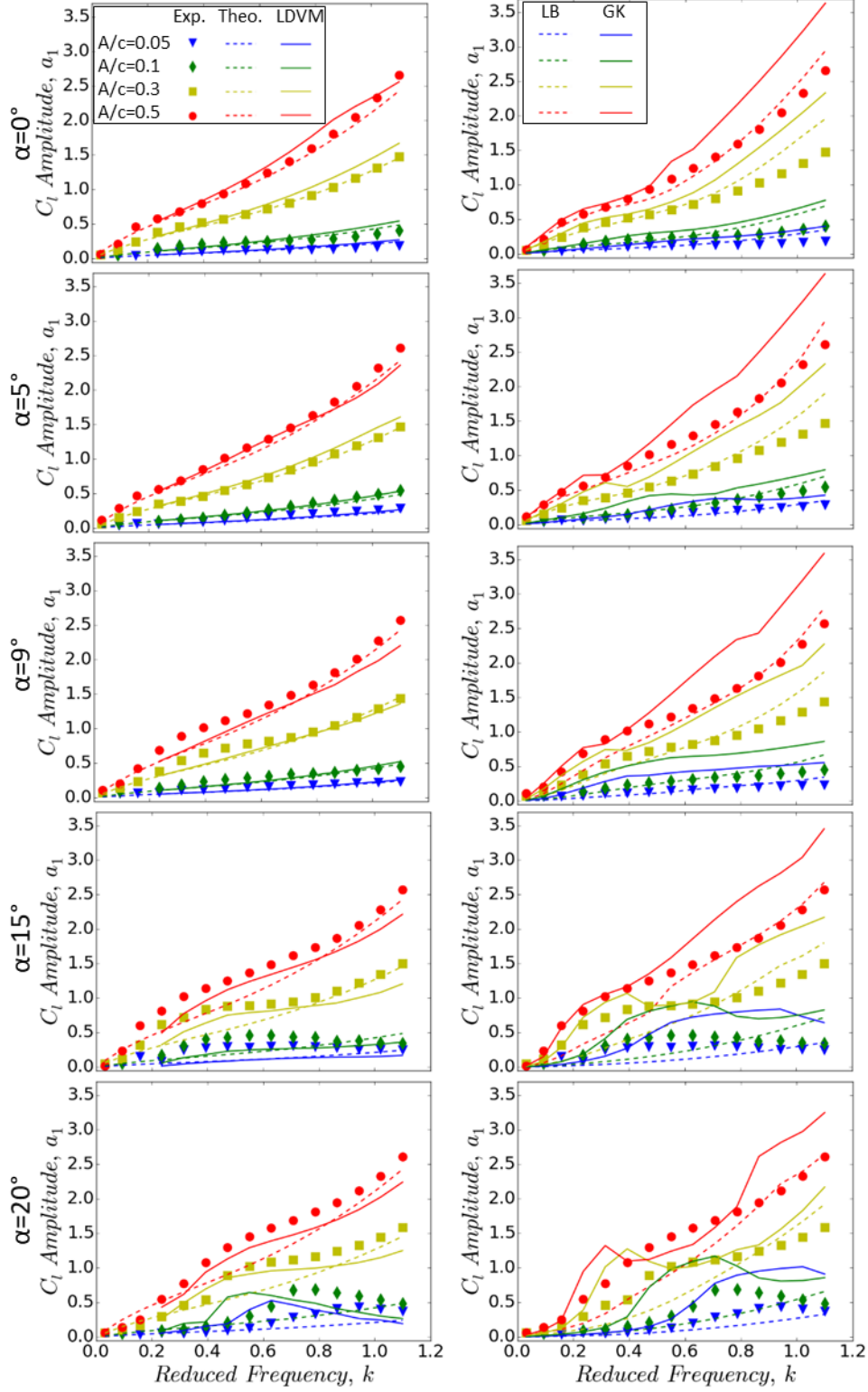
**Figure 9. Lift coefficient amplitude as a function of plunging reduced frequency *k* and amplitude *A/c*, and comparison with Theodorsen and LDVM methods (left), and LB and GK methods (right).**
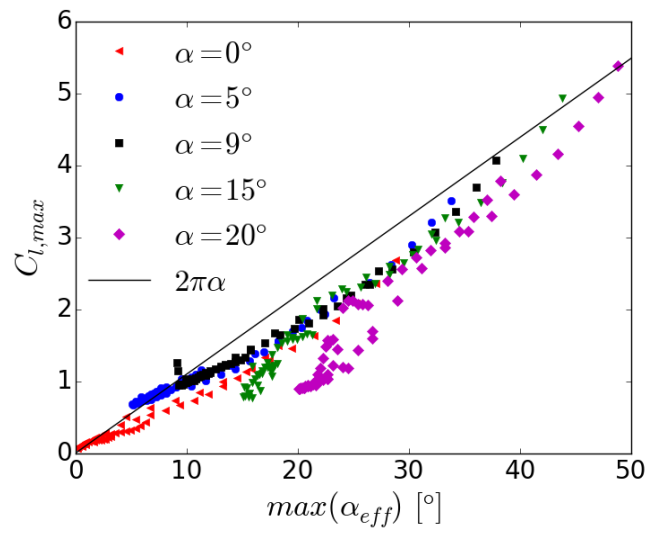
Figure 10. Variation of maximum lift coefficient as a function of maximum effective angle of attack.
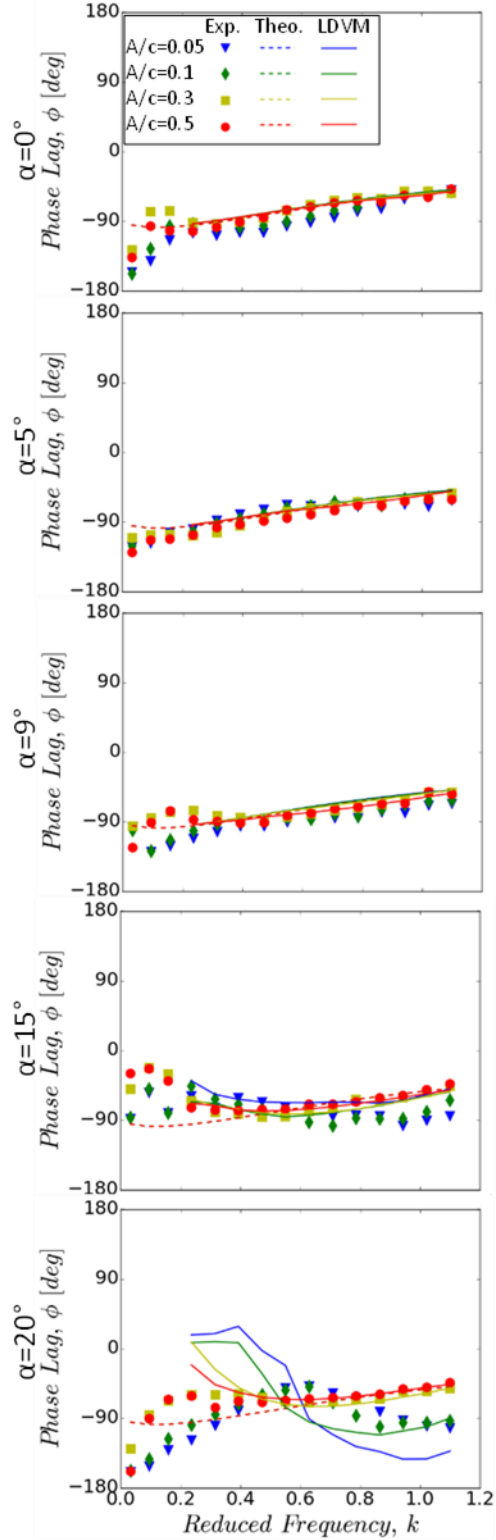
Figure 11. **Variation of lift phase-lag as a function of plunging reduced frequency** *k* **and amplitude** *A/c*, **and comparison with Theodorsen and LDVM methods.**

Figure 12. Phase-averaged lift coefficient (left), and velocity magnitude with streamlines at phase B (*t/T*=0.25) (right) for plunging reduced frequency *k*=0.94 and amplitude *A/c*=0.5.
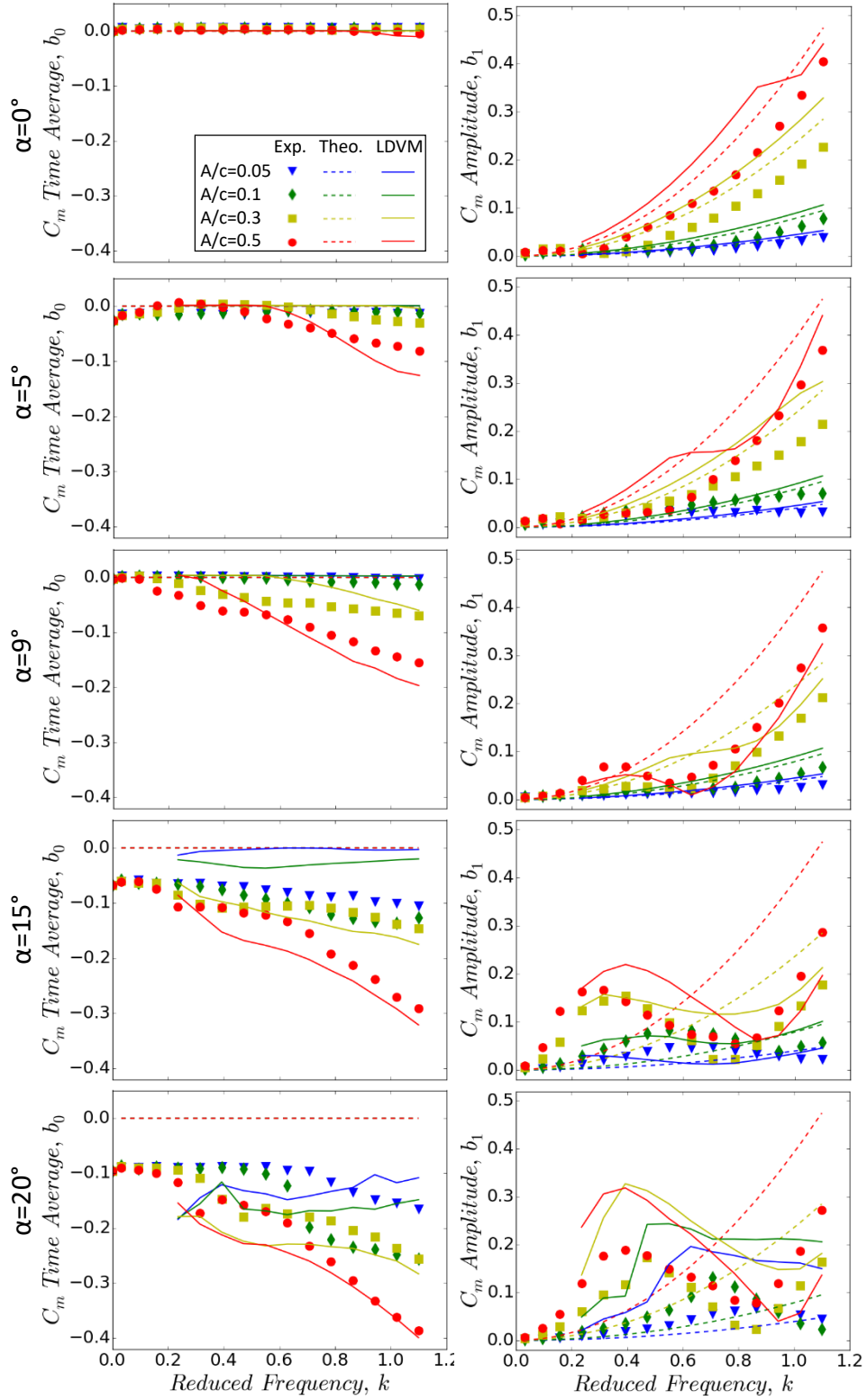
Figure 13. Pitching moment coefficient, mean (left) and amplitude (right), as a function of plunging reduced frequency *k* and amplitude *A/c*, and comparison with Theodorsen and LDVM.
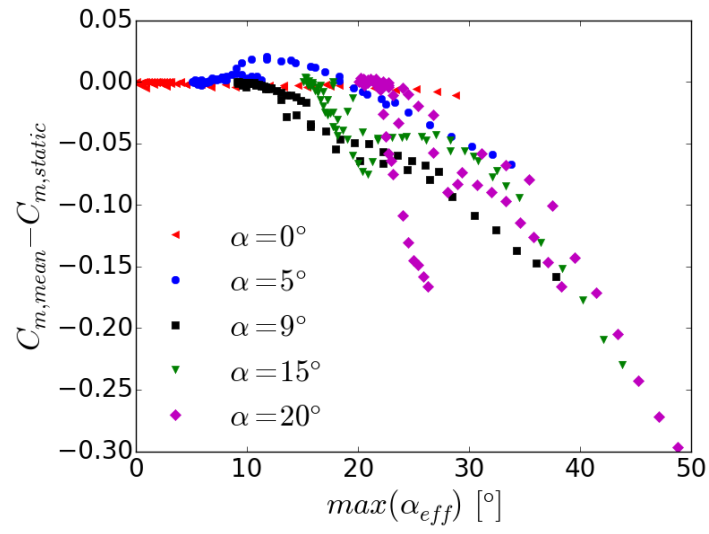
Figure 14. Variation of change in mean pitching moment coefficient as a function of maximum effective angle of attack.
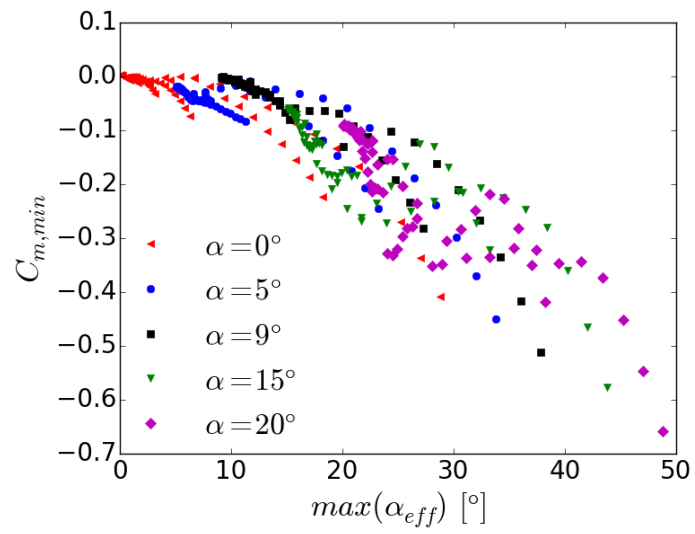
Figure 15. variation of minimum (maximum nose-down) pitching moment as a function of maximum effective angle of attack.
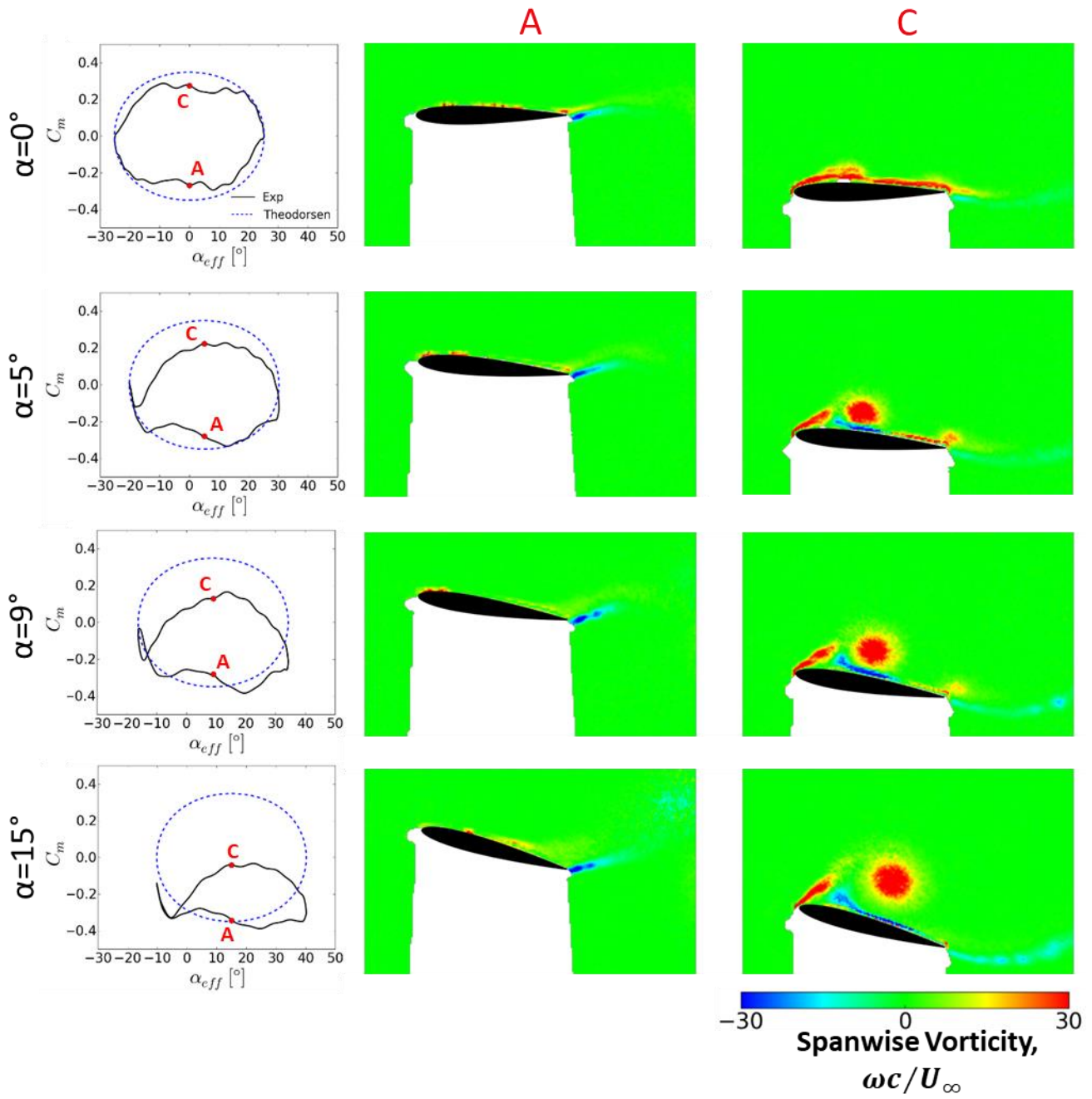
Figure 16. Phase-averaged pitching moment coefficient (left), vorticity at phase A (*t/T*=0.0) (center) and phase C (*t/T*=0.5) (right), for plunging reduced frequency *k*=0.94 and peak-to-peak amplitude *A/c*=0.5.
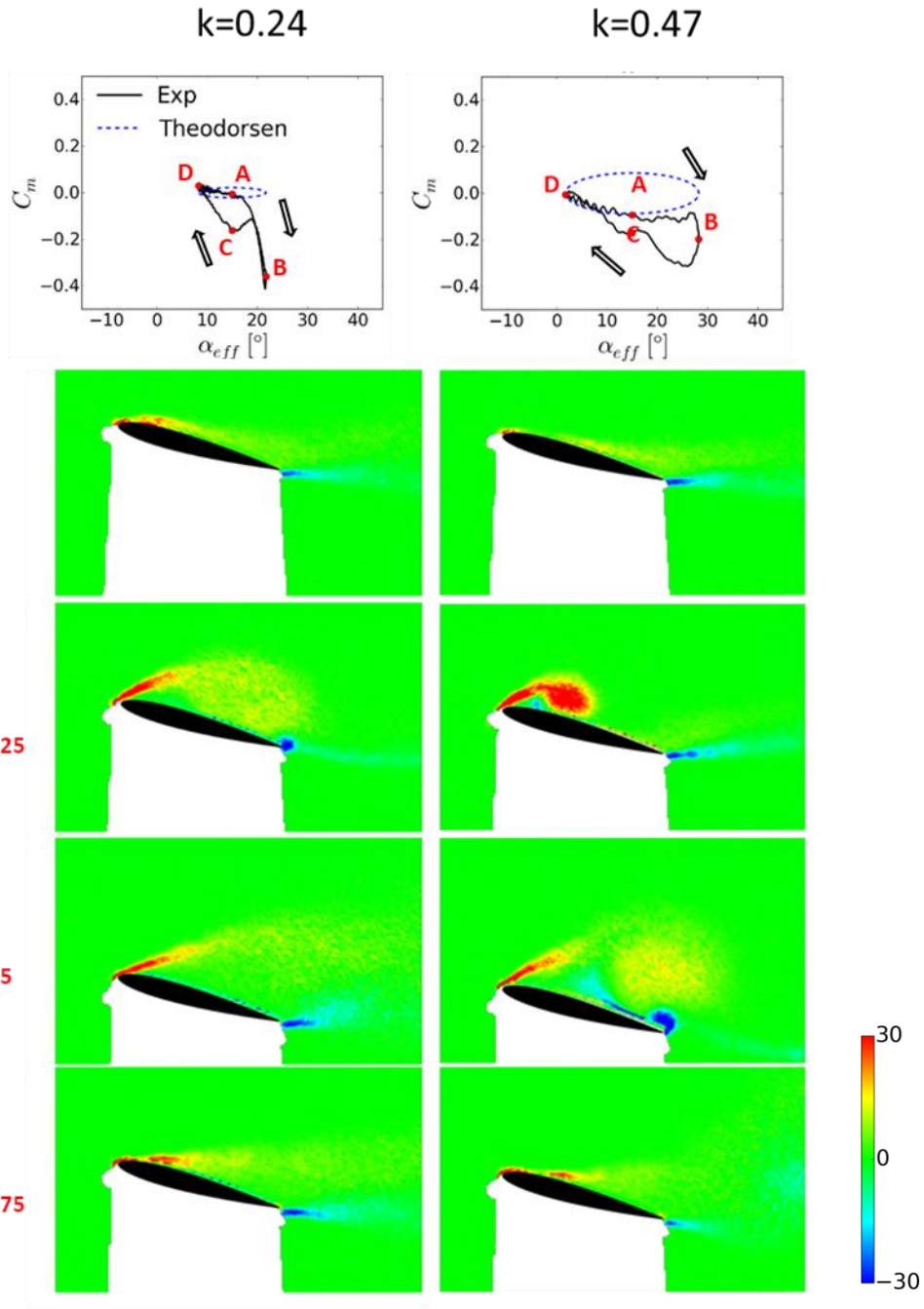
Figure 17. Phase-averaged pitching moment coefficient and spanwise vorticity for α=15°, and plunging peak-to-peak amplitude *A/c*=0.5.